Transport of Surface Freshwater from the Equatorial to the Subtropical North Atlantic Ocean

GREGORY R. FOLTZ, CLAUDIA SCHMID, AND RICK LUMPKIN

NOAA/Atlantic Oceanographic and Meteorological Laboratory, Miami, Florida

ABSTRACT

The transport of low-salinity water northward in the tropical and subtropical North Atlantic Ocean influences upper-ocean stratification, vertical mixing, and sea surface temperature (SST). In this study, satellite and in situ observations are used to trace low-salinity water northward from its source in the equatorial Atlantic and to examine its modification through air–sea fluxes and vertical mixing. In contrast to gridded climatologies, which depict a gradual northward dispersal of surface freshwater from the equatorial Atlantic, satellite observations and direct measurements from four moorings in the central tropical North Atlantic show a distinct band of surface freshwater moving northward from the equatorial Atlantic during boreal fall through spring, with drops in sea surface salinity (SSS) of 0.5–2.5 psu in the span of one to two weeks as the low SSS front passes. The ultimate low-latitude source of the low SSS water is found to be primarily Amazon River discharge west of 40°W and rainfall to the east. As the low-salinity water moves northward between 8° and 20°N during October–April, 70% of its freshwater in the upper 20 m is lost to the combination of evaporation, horizontal eddy diffusion, and vertical turbulent mixing, with an implied rate of SSS damping that is half of that for SST. During 1998–2012, interannual variations in SSS along 38°W are found to be negatively correlated with the strength of northward surface currents. The importance of ocean circulation for interannual variations of SSS and the small damping time scale for SSS emphasize the need to consider meridional freshwater advection when interpreting SSS variability in the tropical–subtropical North Atlantic.

1. Introduction

The role of sea surface salinity (SSS) in tropical mixed layer dynamics and its value for diagnosing changes in Earth's hydrological cycle have received increasing attention in recent years. Observations show positive trends of SSS in the high-salinity subtropics and decreasing trends in the tropics during the past 50 yr (Curry et al. 2003; Cravatte et al. 2009; Durack et al. 2012), consistent with observed changes in precipitation (Wentz et al. 2007; Zhou et al. 2011) and an acceleration of the hydrological cycle predicted under global warming (Held and Soden 2006). Numerous studies have pointed to the importance of near-surface salinity stratification, and particularly the barrier layer phenomenon, for intraseasonal to interannual variations of tropical sea surface temperature (SST) (Vialard and Delecluse 1998; Maes et al. 2002; McPhaden and Foltz

2013) and tropical cyclone intensification (Ffield 2007; Balaguru et al. 2012). Changes in surface freshwater content in the tropical North Atlantic may also affect the ocean's thermohaline circulation through their influence on density and sinking rates in the high-latitude North Atlantic (Vellinga and Wu 2004; Wang et al. 2010).

The usefulness of SSS as an indicator of changes in the water cycle depends on the interplay between the surface moisture flux (evaporation minus precipitation; $E-P$) and mixed layer dynamics, such as horizontal salinity transport and vertical mixing. In regions where $E-P$ dominates, changes in SSS are expected to mirror changes in the hydrological cycle, whereas in regions with strong contributions from mixed layer dynamics, changes in horizontal salinity transport or vertical mixing may complicate the interpretation. In contrast to significant climate change-induced trends in SSS in the Pacific during the past several decades, long-term changes in SSS in the tropical and subtropical Atlantic were found to be insignificant compared to internal variability, suggesting that oceanic processes may have contributed (Terray et al. 2012). Similarly, the mechanisms

Corresponding author address: Gregory R. Foltz, NOAA/Atlantic Oceanographic and Meteorological Laboratory, 4301 Rickenbacker Cswy., Miami, FL 33149.
E-mail: gregory.foltz@noaa.gov

governing barrier layer formation, and the likelihood that barrier layer characteristics will change in the future, depend on $E-P$ and oceanic circulation. A better understanding of the ocean's role in SSS variability in the tropical Atlantic is therefore needed.

The tropical North Atlantic is a region that experiences noticeable seasonal, interannual, and decadal changes in surface salinity (Dessier and Donguy 1994; Grodsky et al. 2014b; Curry et al. 2003). There is a large input of surface freshwater to the tropical North Atlantic Ocean from the combination of rainfall and river outflow, which is then dispersed poleward and mixed downward. The low-latitude input of freshwater in the Atlantic also drives a distinct pattern of near-surface salinity stratification and barrier layer thickness. Thick barrier layers are present in the northwestern basin, where they influence SST and tropical cyclone intensification, and in the central and eastern tropical North Atlantic, where they modulate the seasonal cycle of SST (Pailler et al. 1999; Foltz and McPhaden 2009; Balaguru et al. 2012). Seasonal changes in SSS play a major role in the observed variability of the barrier layer (Mignot et al. 2012).

In the northwestern tropical Atlantic, seasonally varying northwestward transport of low-salinity water from the Amazon exerts a strong influence on SSS. The low-salinity water is advected parallel to the South American coast and toward the Caribbean during boreal winter and spring, when the northwestward North Brazil Current (NBC) is strongest. During summer and fall, a significant portion of the NBC curves eastward away from the South American coast between 5° and 10°N, transporting most of the Amazon's freshwater with it (Figs. 1a,b; Muller-Karger et al. 1988; Lumpkin and Garzoli 2005). As a result, the seasonality of SSS in the northwestern tropical Atlantic is driven mainly by a freshening tendency during the period of strongest northwestward freshwater transport (January–July) and an increasing tendency of SSS during the remainder of the year, when the NBC curves eastward, cutting off the supply of low-salinity water to the northwestern basin (Dessier and Donguy 1994; Reverdin et al. 2007; Foltz and McPhaden 2008; Coles et al. 2013). In contrast, in the ITCZ region, both changes in $E-P$ and horizontal advection are important and undergo strong latitudinal variations (Dessier and Donguy 1994; Foltz et al. 2004; Foltz and McPhaden 2008; Yu 2011; Bingham et al. 2012; Da-Allada et al. 2013). North of the ITCZ, northward transport of lower-salinity water balances an increasing tendency of surface salinity from $E-P$ and entrainment in boreal winter (Johnson et al. 2002; Foltz and McPhaden 2008; Yu 2011).
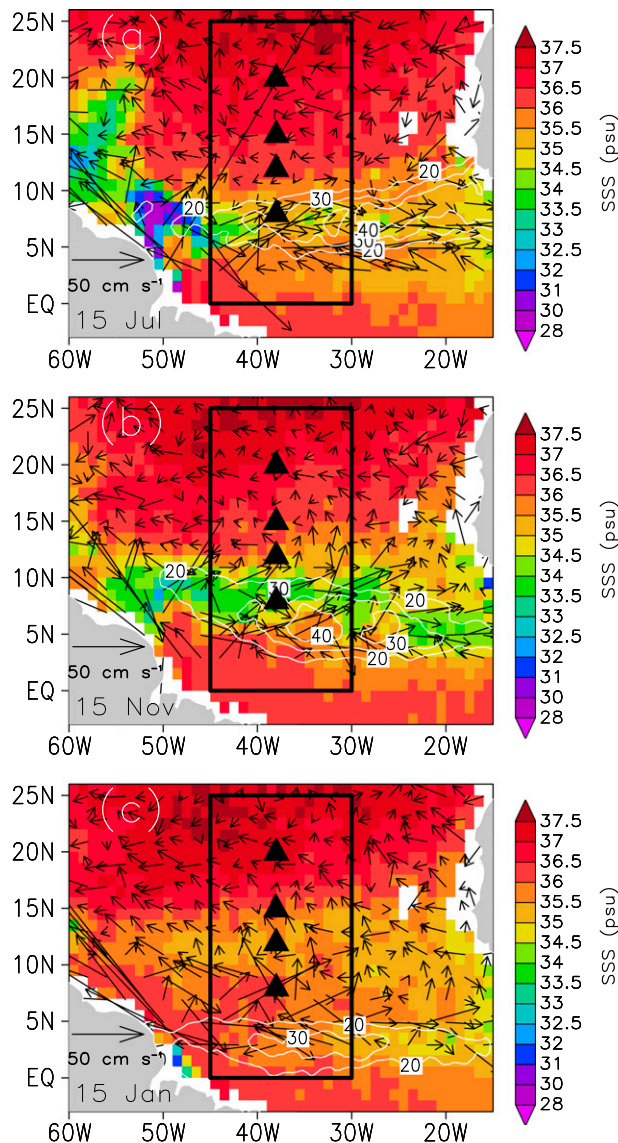

FIG. 1. Weekly SSS from *Aquarius* (shaded), rainfall from TRMM (white contours), and surface currents from a drifter–altimetry synthesis (arrows) centered on (a) 15 July, (b) 15 November, and (c) 15 January in 2012. Black triangles indicate the positions of the PIRATA moorings used in this study. Black rectangle encloses the region used for Fig. 4.

Though several studies have documented the northwestward transport of Amazon outflow toward the Caribbean and its eastward transport during the second half of the year (Muller-Karger et al. 1988; Hu et al. 2004; Coles et al. 2013), the interior pathway of surface freshwater transport from the equatorial to the subtropical North Atlantic, east of the western boundary current, is less well understood. Quantifying this interior transport is important for understanding how changes in freshwater input to the low-latitude source regions are

transmitted to the salinity maximum zone in the sub-tropical North Atlantic (Qu et al. 2011). Previous studies used numerical models or observational analyses based on area averages, specific mooring locations, or monthly global fields. Here, we adopt a different approach, tracing the equatorial low-salinity water northward to assess its low-latitude sources, poleward transport, and modification through air–sea fluxes and oceanic processes.

Through an analysis of available observations, this study addresses several questions related to the northward transport of low-salinity water from the equatorial Atlantic: Does northward freshwater transport occur consistently and steadily throughout the year, or is it more episodic? What is the dominant low-latitude source of freshwater that eventually reaches the subtropics? How does the vertical structure of the low-salinity water change as it travels northward, and how are the changes related to variations in the surface moisture flux and vertical mixing? In contrast to monthly climatologies of SSS, which depict a gradual and steady progression of low-salinity water northward, we show that most of the transport occurs in a distinct pulse of freshwater emanating from the ITCZ and Amazon outflow regions, which is then modified through changes in $E - P$ and vertical mixing along its path to the subtropics.

2. Data and gap-filling procedure

Here, we describe the observational datasets used and the procedure for filling gaps in the spatial and temporal coverage. We use salinity from four moorings of the Prediction and Research Moored Array in the Tropical Atlantic (PIRATA; Bourlès et al. 2008), located at 8°, 12°, 15°, and 20°N along 38°W (Fig. 1). Daily averaged measurements are available during January 1998 through December 2013 at depths of 1, 20, 40, 80, and 120 m at 8°N; 1, 20, 40, and 120 m at 12°N; 1, 5, 10, 20, 40, 60, 80, and 120 m at 15°N; and 1, 10, 20, 40, 60, 80, and 120 m at 20°N. The 20°N mooring is maintained by the United States as part of the PIRATA Northeast Extension, while the other moorings are maintained by Brazil as part of the original PIRATA array. Suspicious salinity data at a depth of 10 m during August 2011–January 2013 were removed from the 20°N record. Daily averaged subsurface temperature, with 20-m vertical resolution in the upper 120 m and generally 5- to 10-m resolution in the upper 20 m, is used with salinity to calculate the mixed layer depth. Precipitation, wind speed, SST, relative humidity, and air temperature from the moorings were obtained to compute the surface freshwater flux described in section 3.

Argo profiles of temperature, salinity, and pressure, with typical vertical resolutions of 5 m, were used to fill gaps in the PIRATA mooring time series of temperature and salinity and to provide a broader context for the results based on the mooring data. In addition, daily satellite retrievals of precipitation are available from the Tropical Rainfall Measuring Mission (TRMM) on a 0.5° × 0.5° grid for the period December 1997 to December 2013. Daily surface salinity from the Aquarius satellite instrument was obtained for the period August 2011 through December 2013 on a 1° × 1° grid. Gaps in time, because of the weekly repeat cycle of Aquarius, were filled with linear interpolation. We also use SSS data from the individual satellite passes, which have a typical meridional resolution of 0.1° and a zonal resolution of 0.02° along the pass. Each pass has measurements from the satellite's three footprints. Here, we use the mean value from all footprints at each location along the pass.

Surface evaporation was obtained from the OAFlux product, which is available for January 1985–September 2013 on a 1° × 1° grid (Yu and Weller 2007). The satellite precipitation and SSS data, combined with OAFlux evaporation and mixed layer depth from temperature and salinity profiles, are used to calculate the surface flux contribution to changes in SSS across the tropical North Atlantic. A monthly climatology of near-surface currents on a 1° × 1° grid from surface-drifting buoys (Lumpkin and Johnson 2013) and a weekly drifter–altimetry synthesis product on a ⅓° × ⅓° grid for the period October 1992–August 2013 (Lumpkin and Garzoli 2011) are used in calculations of meridional freshwater advection and transport.

Analysis of meridional salinity transport in the upper ocean on submonthly time scales requires observations of near-surface salinity with high temporal and vertical resolutions. We therefore rely on profiling float data from Argo, with a typical vertical resolution of 5 m in the depth range we consider, and measurements from PIRATA moorings, which are available as daily averages but at a lower vertical resolution compared to Argo. These two datasets are combined to take advantage of the strengths of each. First, a daily time series of near-surface salinity is created at each mooring location using only the data from the mooring. The time series at a depth of 1 m (S_{1m}) are used, and gaps are filled with salinity from the next deepest level (S_{deeper}) after seasonal bias correction. For the seasonal bias correction, the difference between S_{deeper} and S_{1m} is first calculated, and a daily climatology of the difference is created using all available data. This daily climatology, repeated for each year, is then subtracted from the daily time series of S_{deeper}, and the bias-corrected S_{deeper} is used to fill gaps
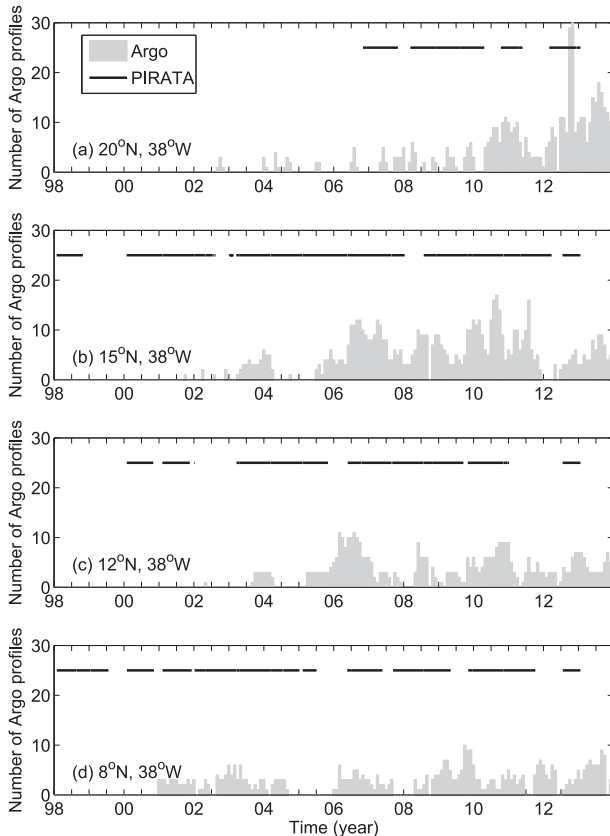
FIG. 2. Availability of PIRATA-analyzed SSS (black lines) and number of Argo profiles within a 2° × 2° box centered on the mooring location (gray bars, one for each month) during 1998–2013. The moorings are located at (a) 20°, (b) 15°, (c) 12°, and (d) 8°N, along 38°W.

in S_{1m}. If gaps remain after filling with S_{deeper}, the procedure is repeated for each successively deeper level down to 20 m. A depth of 20 m is used since salinity at this depth is still highly correlated with salinity at a depth of 1 m (correlation coefficient of 0.85 for a combined time series of all daily data from all four moorings). If there are no salinity measurements in the upper 20 m on a given day, the gap is not filled. Figure 2 shows the availability of surface salinity at each mooring location after the gap-filling procedure.

Next, salinity profiles from all Argo floats within ±2° of latitude and longitude from a given PIRATA mooring are used to create a lookup table for subsurface salinity down to 120 m as a function of Argo salinity at a depth of 10 m and for a calendar month. Figure 2 shows the number of Argo profiles available for the lookup table in each 2° × 2° box centered on each PIRATA mooring. The Argo coverage is generally greatest from 2006 onward at 8°, 12°, and 15°N and from 2010 onward at 20°N. A "first-guess" daily time series of salinity, from

10 m down to 120 m with a 5-m vertical resolution, is then created at each mooring location using the daily time series of near-surface salinity from the mooring and the Argo lookup table for the subsurface profile. Using this first-guess salinity time series and the PIRATA salinity time series with its original vertical resolution, optimum interpolation (with an exponential depth scale of 20 m) is used to create a daily time series of "analyzed salinity" in the upper 120 m at each mooring location. The advantage of this technique is that the original daily resolution of the mooring time series is retained while significantly improving the vertical resolution. These qualities are advantageous for tracking the arrival of the low-salinity water and for calculating depth-dependent meridional freshwater transport.

For a consistency check on the results from the PIRATA-analyzed salinity and to calculate salinity transport between the moorings, we also create a gridded Argo salinity product for each calendar month on a 1° × 1° using optimum interpolation with a horizontal scale of 3°. The vertical resolution of the gridded Argo product is 10 m.

3. Methodology

The methodology for computing the northward transport of freshwater from the equatorial to the subtropical North Atlantic, using a combination of satellite, Argo, and surface drifter data, is presented first, followed by the methodology used to calculate freshwater transport and vertical mixing from the PIRATA time series.

a. Satellite, Argo, and surface drifters

The rate of change of mixed layer salinity can be expressed as

$$\frac{\partial S}{\partial t} = \frac{(E - P)S}{h} + \epsilon. \tag{1}$$

Here, S is salinity averaged from the surface to the base of the mixed layer in nondimensional units (i.e., $kg\,kg^{-1}$), estimated using the gridded *Aquarius* SSS retrievals; E is evaporation from the OAFlux product; P is precipitation from TRMM; and h is the mixed layer depth, calculated using the criterion of a $0.1\,kg\,m^{-1}$ increase in density from a depth of 10 m. Previous studies have shown that SSS is highly correlated with S (e.g., Foltz et al. 2004). Individual Argo profiles are first used to calculate h, and then the values are interpolated horizontally for each calendar month using optimum interpolation as described in the previous section. The ϵ term represents the sum of horizontal salinity advection,

vertical processes such as entrainment and turbulent mixing, and errors in the calculation of the other terms in (1).

A daily time series of the SSS driven by the surface moisture flux [first term on the right in (1)] is created at each grid point by integrating (1) in time:

$$S_{\text{flux}}(t) = S(t_0) + \int_{t_0}^{t} \frac{(E-P)S}{h} dt'. \tag{2}$$

A date of 25 August 2011 is used for t_0, and t then varies from 26 August 2011 to 14 June 2012, starting with the observed $S(t_0)$. This gives a ~10-month time series of S_{flux} at each grid point. Similarly, time series are generated for 15 June 2012–14 June 2013 and for 15 June 2013–25 December 2013. These individual time series are then combined to form a full record of S_{flux} during 25 August 2011 through 25 December 2013. The starting dates of 15 June in 2012 and 2013 and 25 August in 2011 ensure that the large drops in SSS between 5° and 10°N (Figs. 1a,b) are captured early in the time integration, before potential biases in the E, P, and h products can exert a large influence on $S(t)$. Note that this method can result in large and discontinuous jumps in S_{flux} between the end of one integration period and the start of the next, since only $E - P$ is used to force SSS.

The portion of the SSS on a given day that is driven by oceanic processes (e.g., horizontal advection and vertical mixing) can then be approximated as

$$S_{\text{resid}}(t) = S(t) - S_{\text{flux}}(t). \tag{3}$$

Here, $S(t)$ is the observed SSS from *Aquarius* on a given day. Note that S_{resid} is "reset" on 15 June in 2012 and 2013, when the time integration in (2) begins from a new $S(t_0)$. Here, and in the equations that follow, S is given in nondimensional units. Equation (3) gives estimates of the oceanic contribution to SSS at each grid point during the period 25 August 2011–25 December 2013, when *Aquarius* data are available.

The *Aquarius* instrument measures salinity in the upper ~2 cm, which may not always represent the depth-averaged salinity in the upper 20 m. To calculate the seasonal cycle of meridional freshwater transport directly, we therefore rely on Argo data. First, the freshwater content in certain depth and longitude ranges at a given latitude are calculated:

$$F = \frac{\rho_o}{\rho_f \Delta \phi} \int_{45°W}^{30°W} \int_0^{20} (1-S) \, dz \, d\phi. \tag{4}$$

Here, ρ_o is the density of seawater, ρ_f is the density of freshwater, S is the salinity (mass of salt per mass of seawater), 30° and 45°W are the zonal boundaries of the region (ϕ is longitude), and the surface and 20 m are the

vertical boundaries. This equation gives the freshwater content in the upper 20 m, averaged between 30° and 45°W. The objectively analyzed monthly climatology of Argo salinity is used for S. The meridional freshwater transport is then calculated from (4) as $T = Fv$, where v is near-surface velocity from the surface drifter monthly climatology. Because the drifter climatology gives velocity at an average depth of 15 m, and salinity is nearly uniform in the upper 20 m in the region we consider, we chose to calculate the meridional freshwater transport only in the upper 20 m.

b. PIRATA moorings

The same methodology [(1)–(3)] is used to calculate the mixed layer salinity budget components at the PIRATA mooring locations. One of the main differences is that instead of daily time series at each 1° grid point, daily time series are created only at 8°, 12°, 15°, and 20°N along 38°W. The other difference is that instead of using satellite and Argo data, we use direct measurements from the moorings for evaporation and precipitation and the combined Argo–PIRATA product for salinity. The daily time series of Argo–PIRATA-analyzed SSS from each mooring are used to calculate S_{flux} and S_{resid} in (2) and (3). Precipitation is available directly from the moorings, and gaps are filled using TRMM daily averages. The surface latent heat flux is calculated from version 3 of the Coupled Ocean–Atmosphere Response Experiment (COARE) algorithm (Fairall et al. 2003) using daily SST, wind speed, relative humidity, and air temperature from the moorings. The latent heat flux is then converted to evaporation as $E = Q_e/(\rho_f L_e)$, where Q_e is the surface latent heat flux, ρ_f is the density of freshwater (1000 kg m^{-3}), and L_e is the latent heat of vaporization (2.355 × 10^6 J kg^{-1}). Gaps in PIRATA evaporation are filled with daily data from OAFlux. The mixed layer depth is calculated using daily temperature and analyzed salinity from each mooring based on the criterion of a 0.1 kg m^{-3} density increase from a depth of 1 m.

One of the main advantages of the mooring time series is their daily resolution, which enables better tracking of low-salinity water as it moves northward to the subtropics, compared to weekly or monthly averages from *Aquarius* or Argo. From the daily mooring time series of salinity, the meridional transport of freshwater along 38°W is calculated based on the observed drop in salinity during the arrival of the low SSS front. This method is chosen because of the short time period over which the drop in SSS occurs (typically a decrease in SSS of about 2 psu in less than 15 days), which makes the arrival of the low SSS front easy to identify and ensures that surface fluxes and vertical mixing do not spuriously contribute significantly to the decrease in SSS. For

a given drop in salinity, the amount of freshwater that was added to create the drop can be calculated as

$$V_f = \frac{V_1[(1 - S_2)\rho_2 - (1 - S_1)\rho_1]}{\rho_f - \rho_1(1 - S_1)}. \quad (5)$$

Here, V_f is the volume per unit area (i.e., depth) of freshwater that is added; S_1 and S_2 are the initial and final depth-averaged salinity, respectively; ρ_1 and ρ_2 are the initial and final density, respectively (density is a function of temperature from the mooring and salinity from the mooring-Argo analysis); V_1 is the initial volume of seawater; and ρ_f is the density of freshwater. Equation (5) follows from the continuity equation for salt. For the simple case in which $\rho_1 = \rho_2$, the amount of freshwater added is proportional to the magnitude of the drop in salinity ($S_1 - S_2$) and inversely proportional to the initial salinity S_1. For the case of constant $S_1 - S_2$, the inverse proportionality to S_1 occurs because as S_1 increases, the amount of freshwater removed from the water column decreases and hence the amount that must be added is lower. The timing and magnitude of the salinity drops are calculated from the daily analyzed salinity time series at each mooring, after smoothing with a 5-day running-mean filter. For each year at each location, the maximum SSS is identified using the 120-day period prior to the SSS minimum, and the salinity drop is calculated as the salinity on the day of the SSS maximum minus the salinity on the day of the SSS minimum.

4. Results

In this section, we first examine the mixed layer salinity budget and meridional freshwater transport in the tropical North Atlantic using satellite and Argo data. The freshwater transport and its modification through $E - P$ and vertical mixing are then quantified using PIRATA data. Finally, we briefly discuss interannual variability of the northward surface freshwater transport.

a. Salinity budget and freshwater transport

Seasonal variability of SSS in the tropical North Atlantic is influenced by freshwater discharge from the Amazon River and its lateral dispersal, changes in evaporation and precipitation associated with seasonal variations of the ITCZ, and turbulent mixing of higher-salinity water into the surface mixed layer. The lowest values of SSS in the tropical North Atlantic are found in the northwestern basin and in a zonal band under the ITCZ, consistent with northwestward and eastward advection of Amazon outflow, respectively, and high rainfall in the ITCZ (Fig. 1; Dessier and Donguy 1994). A pronounced shift in the location of the lowest-salinity
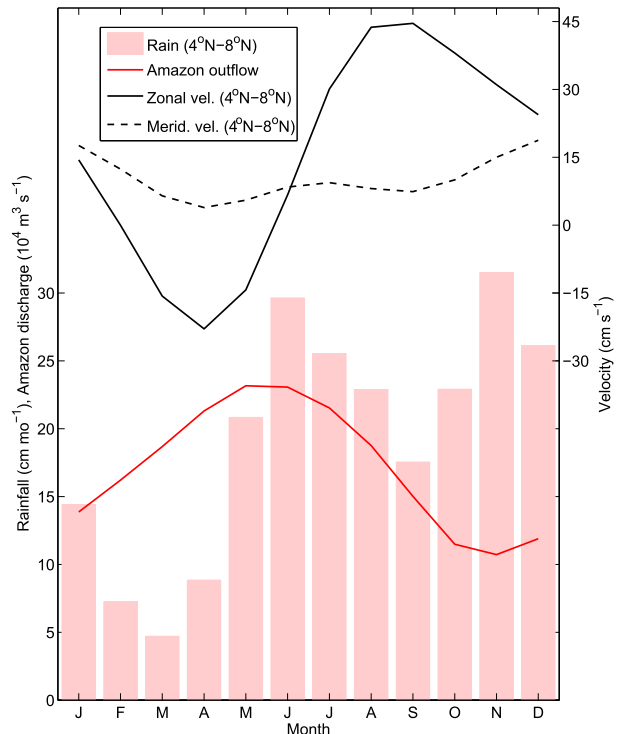

FIG. 3. Monthly climatological rainfall (pink bars), Amazon River discharge (red line), zonal surface velocity (solid black), and meridional surface velocity (dashed black). Rainfall and velocity are averaged between 4° and 8°N, 30° and 45°W.

water occurs during boreal summer and fall. In July, a large area of low-salinity water can be seen extending northwestward from the mouth of the Amazon, consistent with the direction of the mean surface currents (Fig. 1a). By November, the low-salinity water has relocated to the western ITCZ region (5°–10°N and west of 35°W), where the North Equatorial Countercurrent (NECC) is well established and rainfall is high (Fig. 1b). By January, the band of low-salinity water has weakened considerably and expanded northward in the central and western basin (Fig. 1c).

There are several factors that may contribute to the changes in SSS in the central tropical North Atlantic (30°–45°W) beginning in boreal summer. In the near-equatorial region (4°–8°N), rainfall increases dramatically leading up to boreal summer from 5 cm in March to 30 cm in June (Fig. 3). Amazon outflow reaches a maximum of $2.3 \times 10^5 \, \mathrm{m^3 \, s^{-1}}$ in May–June, which is twice as much as in October–December (Fig. 3). During July–January, the excess freshwater from the Amazon and ITCZ rainfall is transported eastward by the NECC at speeds of $15–45 \, \mathrm{cm \, s^{-1}}$, contributing to the eastward expansion of the freshwater visible in Fig. 1. Throughout the year there is a northward component to the surface
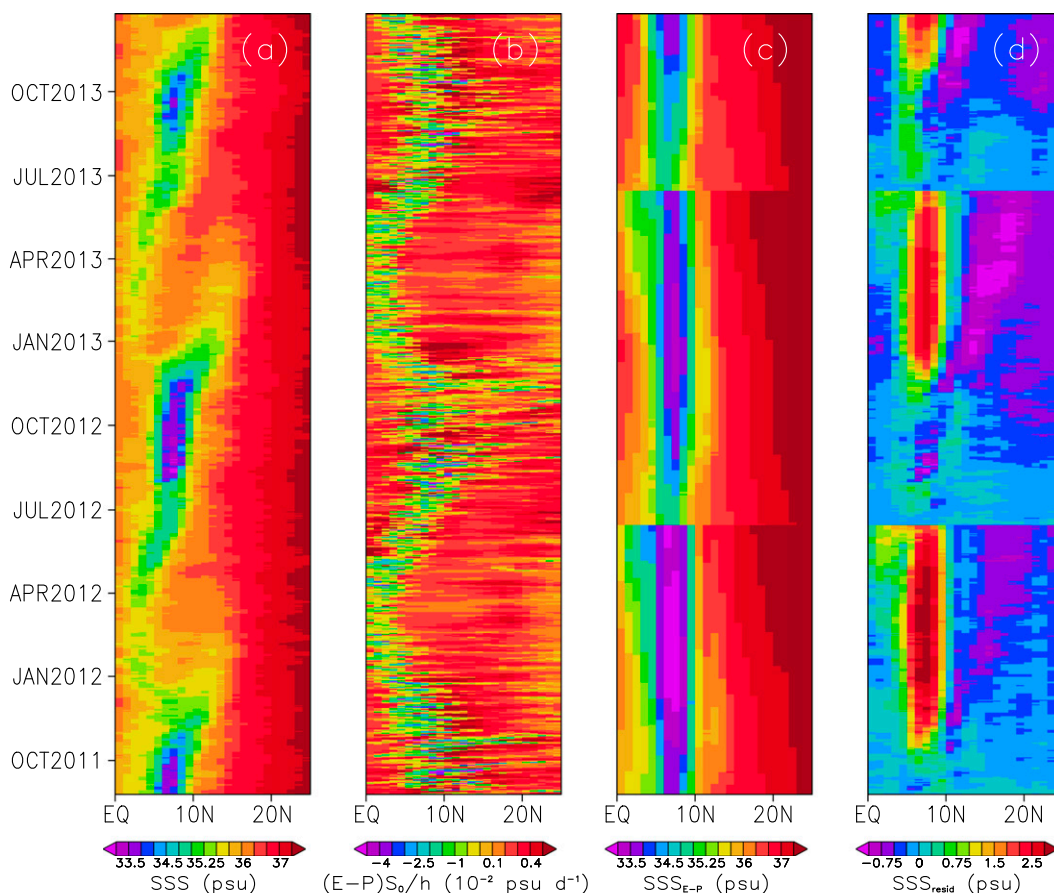
FIG. 4. Daily (a) *Aquarius* SSS, (b) rate of change in SSS due to $E-P$, (c) integrated SSS due to $E-P$ [i.e., the time integration of (b) from June of one year to June of the following year], and (d) difference between (a) and (c), showing changes in SSS due to factors such as horizontal advection. Plots are shown for the period August 2011–December 2013, averaged between 30° and 45°W.

currents in the 4°–8°N band, tending to disperse low-salinity water from the equatorial region northward. Beginning in October, the northward currents increase in strength as the ITCZ moves southward and the trade winds intensify. The increase in meridional velocity is consistent with the northward progression of the lowest-salinity water from ~8°N in November to ~12°N in January (Figs. 1b,c).

For a more quantitative analysis of the factors affecting SSS in the central tropical North Atlantic, we turn to latitude–time plots of the mixed layer salinity budget averaged between 30° and 45°W (Fig. 4). Strong seasonality in SSS is evident, with the lowest values near 8°N during July–December and 0°–5°N during January–June (Fig. 4a). A pronounced minimum occurs during August–November, consistent with the seasonal cycles of rainfall, Amazon outflow, and ocean circulation (Fig. 3). The seasonal cycle of SSS generally agrees with that of $E-P$, which shows the strongest negative values (i.e., heavy rainfall) generally during August–November

and between 5° and 10°N (Fig. 4b). During January–June, the ITCZ, and with it the region of heaviest rainfall, is located farther south. The seasonal cycle of E–P reproduces observed SSS reasonably well north of about 15°N but cannot explain the strong seasonality in SSS to the south (Fig. 4c). Negative values of E–P account for a large portion of the decrease in SSS during July–October, but beginning in November the residual, consisting mainly of horizontal advection and vertical mixing, dominates the seasonal cycle of SSS between 5° and 20°N (Fig. 4d). Most noticeable is a strong increase in SSS between 5° and 10°N that is most likely caused by horizontal advection (i.e., Grodsky et al. 2014a) and a northward-propagating freshening tendency from advection between 10° and 20°N that is particularly well defined during December 2012–April 2013.

To put the salinity budget in the central tropical North Atlantic in perspective, we consider the role of the salinity budget residual for the entire tropical North Atlantic during two distinct periods: July–October, when

the low-salinity water is expanding eastward and intensifying between 5° and 10°N, and November–February, when northward propagation of the low-salinity band is evident. Between July and October, SSS decreases by 1–2.5 psu in the NECC region (40°–50°W) and increases by a similar amount northwest of the Amazon's mouth (Fig. 5a). The residual accounts for a large fraction of these changes (Figs. 5b,c). To the east of 35°W and between 7° and 12°N, the change in SSS is a small residual between a strong freshening tendency from rainfall and a positive SSS tendency from the combination of horizontal advection and vertical mixing. Outside of these regions, the July–October changes in SSS are much smaller, and the role of oceanic processes is therefore less certain.

Between November and February, SSS decreases between 12° and 17°N east of 50°W and increases in the NECC region and in the far western basin (Fig. 5d). The increases in SSS are consistent with the decrease in eastward flow of the NECC and the seasonal minimum in Amazon outflow during September–February (Figs. 3, 5d). The decrease in SSS to the north of the NECC is consistent with the northward propagation of the low-salinity signal from the NECC region. Indeed, the salinity budget residual explains most of the SSS changes observed during November–February (Figs. 5e,f). Individual satellite passes from *Aquarius* show more clearly the progression of the low SSS water northward beginning in November (Fig. 6a). A pronounced SSS minimum of 33 psu is present at 8°N in October. During November–April the low SSS water moves northward and weakens, though in April there is still a noticeable SSS minimum, with a sharp increase in SSS northward from 20°N.

Consistent with the importance of northward advection inferred from the mixed layer salinity balance and *Aquarius* passes, there is a noticeable northward progression of the maximum in 0–20-m freshwater content in the central tropical North Atlantic (30°–45°W) from 7°N in September to 13°N in January (Fig. 6b). In contrast, the latitude of maximum northward freshwater transport increases very little during the same time period, from 4°N in September to 6°N in January (Fig. 6c). This is mainly because the meridional distribution of freshwater transport is controlled primarily by the surface currents, which are strongest between 4° and 6°N. The location of the strongest northward currents is consistent with the fastest northward propagation of SSS and freshwater content during September–November and weaker propagation during November–January. The sharp decrease in meridional salinity transport north of 6°N will tend to create a zonally oriented salinity front, which then is advected northward by the surface currents. Results from the PIRATA time series in the next section show the advection of this front more clearly. Note that at most latitudes, freshwater content in the upper 20 m increases between September and January, primarily because of a decrease in temperature and hence an increase in density [Fig. 6b and Eq. (4)].

In summary, satellite SSS data show a strong decrease in SSS in the 5°–10°N band of the western Atlantic during boreal summer through fall. A simple salinity budget analysis suggests that the decrease in SSS to the west of 40°W is driven primarily by eastward transport of low SSS Amazon water, while to the east it results mainly from enhanced rainfall associated with the location of the ITCZ. The Amazon- and rainfall-induced low SSS water progresses northward to 15°–20°N during boreal fall through spring, consistent with advection by northward near-surface currents.

b. Freshwater transport and vertical mixing from PIRATA

To investigate the northward freshwater transport in more detail and to estimate the vertical mixing-induced damping of the low-salinity water, in this section we analyze data from four PIRATA moorings along 38°W. The main advantage of the moorings is their daily resolution, compared to the weekly repeat cycle of *Aquarius* and uneven spatial and temporal coverage from Argo. The moorings, located at 8°, 12°, 15°, and 20°N, are well positioned to capture the strong zonal band of surface freshening centered near 8°N as well as its subsequent northward transport (Fig. 1).

At 8°N, SSS changes very little during January–May, with an average value of about 36 psu (Fig. 7a). From June to October, SSS decreases by 2–5 psu. There is considerable interannual variability in the minimum SSS, ranging from 31 psu in 2009 to 34 psu in 2007. On average, oceanic processes, estimated from the salinity budget residual, tend to increase SSS during June–December. The increase is likely due in large part to horizontal advection, given the mooring's position near the center of the zonally oriented low SSS band and mean northward surface currents (Fig. 1). The mooring at 8°N is also located near the easternmost extent of the Amazon plume so that eastward advection of its low SSS water is generally weak (Figs. 5b, 7a). The pronounced drop in SSS here during June–October is therefore driven primarily by enhanced rainfall and balanced by horizontal advection, though in some years eastward advection of the Amazon's low SSS plume appears to be important, as demonstrated by sharp drops in the residual-driven SSS (i.e., 2001, 2003, 2009, and 2011). This conclusion is consistent with results from the larger-scale analysis presented in the previous section and the modeling results of Coles et al. (2013).
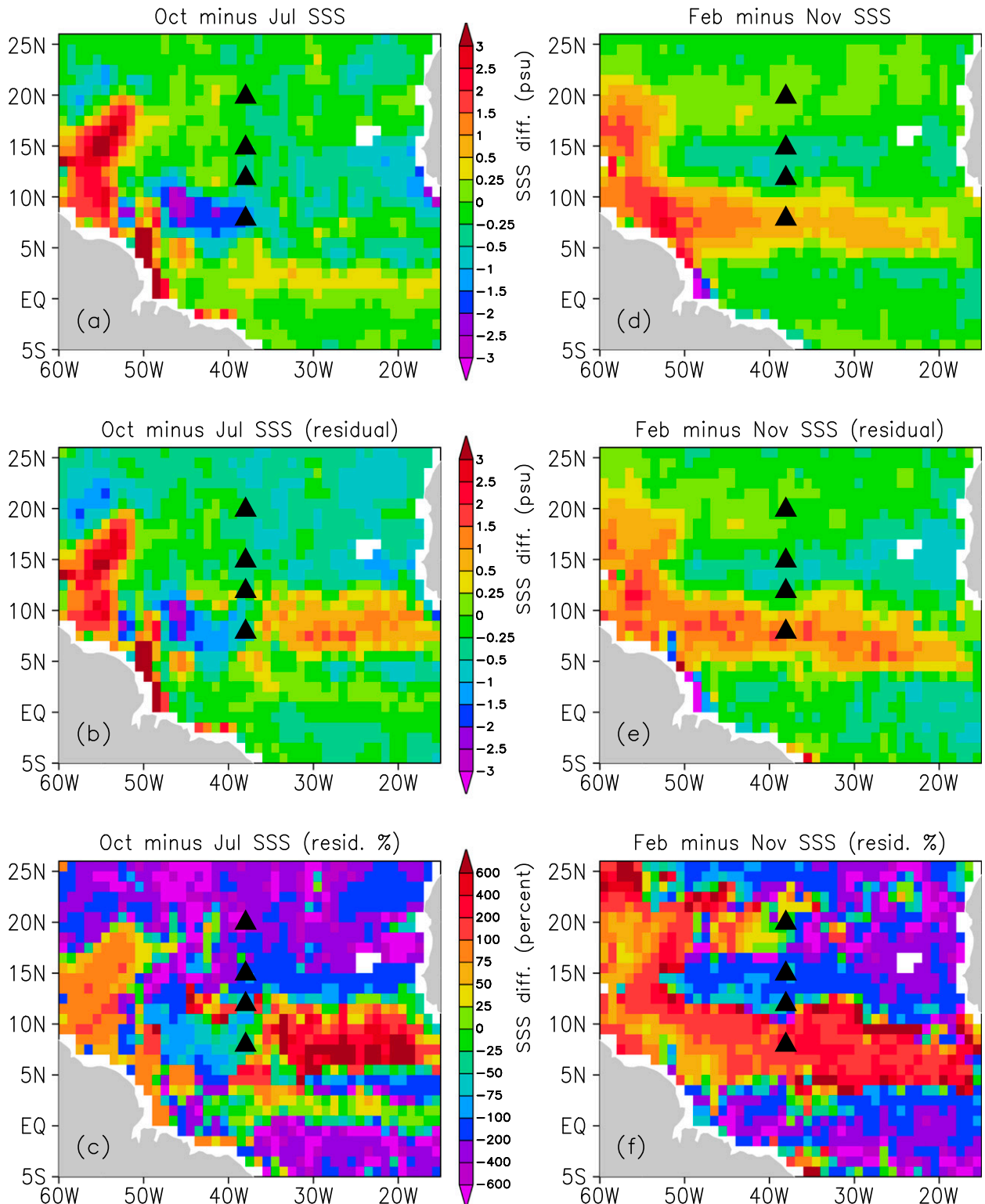
FIG. 5. (a) Difference between SSS in October 2012 and July 2012. (b) As in (a), but for SSS due to horizontal advection. (c) As in (a), but for the percentage of SSS change that is due to horizontal advection. Positive values in (c) indicate an increasing tendency of SSS due to advection; negative values indicate a decreasing tendency. (d)–(f) As in (a)–(c), but for the difference between February 2013 and November 2012.
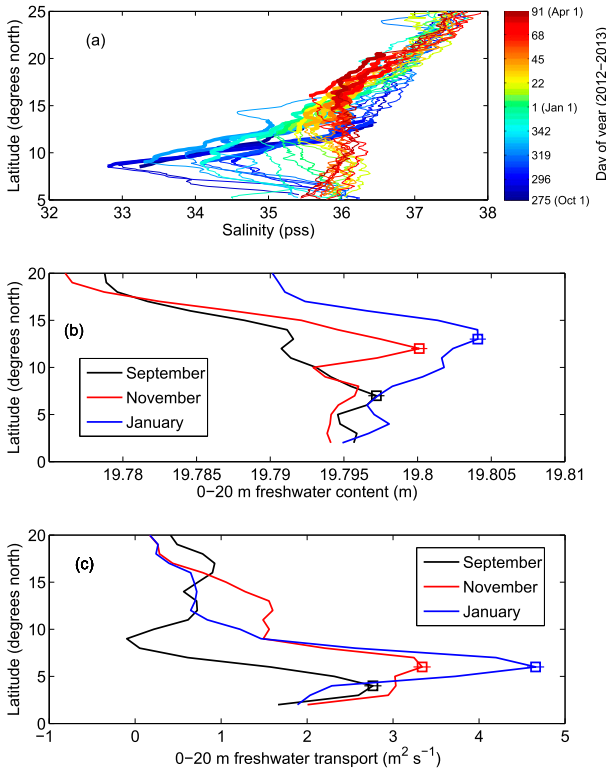
FIG. 6. (a) SSS from *Aquarius* satellite passes during October 2012–April 2013 that were located in the longitude range 36°–40°W between 5° and 25°N. Color indicates time of year. Thick portions of lines highlight the ~5° of latitude north of the salinity minimum for that pass, emphasizing sharp increases in SSS. (b) Climatological freshwater content in the upper 20 m from Argo, averaged between 30° and 45°W and shown for September (black), November (red), and January (blue). Squares indicate the maximum value for each segment. (c) As in (b), but for meridional freshwater transport in the upper 20 m, calculated from Argo and surface drifters. Horizontal lines centered on squares in (b) and (c) indicate one standard error.

At 12°N, almost all of the seasonal variations in SSS can be explained by horizontal advection, estimated from the salinity budget residual (Fig. 7b). SSS decreases by 1–2.5 psu between June and November–December, about half of the magnitude of the decrease observed at 8°N. The drop in SSS at 12°N normally occurs in less than two weeks, whereas at 8°N the decrease is often spread out over a period of several months. The abrupt drop in SSS at 12°N is consistent with the northward advection of a low SSS front from 8° to 12°N that contains a sharp front at its leading edge. The more gradual decrease in SSS at 8°N supports the conclusion that enhanced rainfall plays a larger role here, since the time-integrated effect of rainfall is more slowly evolving compared to that of a northward-moving front.

The low SSS front arrives at 15°N during December–January in most years and the observed front is less
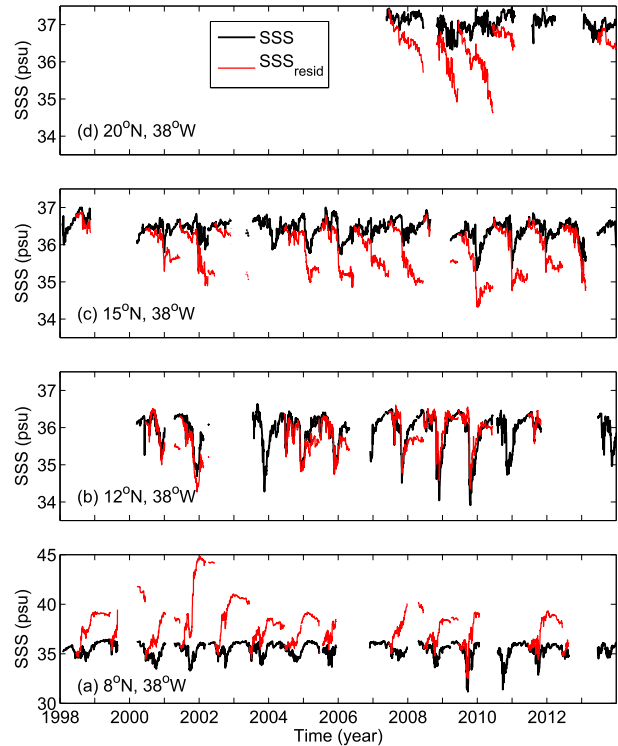

FIG. 7. Daily time series of the PIRATA-analyzed SSS (black) and estimates of SSS due to oceanic processes such as horizontal advection (red), obtained from the time integration of the salinity balance residual from June of one year to June of the following year. Values are shown during 1998–2013 at (a) 8°, (b) 12°, (c) 15°, and (d) 20°N along 38°W. Note that (a) is the bottom panel.

intense compared to 12°N, with a drop in SSS of 0.5–1 psu on average at 15°N (Fig. 7c). The drop in SSS generally occurs within a period of one or two weeks, consistent with the timing at 12°N. In contrast to the results at 12°N, however, at 15°N horizontal advection tends to lower SSS throughout the year, even before the arrival of the low SSS front and to a lesser extent after its arrival. The stronger increasing tendency of SSS due to E–P at 15°N is consistent with higher evaporation and lower precipitation at 15°N compared to 12°N (Foltz et al. 2004).

By 20°N the low SSS front, defined by the observed drop in SSS, has weakened substantially, and its arrival is more difficult to discern in the SSS time series (Fig. 7d). Drops in SSS of about 0.5 psu or less are evident in April 2009 and 2010 and to a lesser extent in April 2013. Though the time series at this location is much shorter, the consistency in the timing and magnitude of the SSS drop during the 3 yr that are available suggests that they are likely to be caused by the same low SSS front that originated at 8°N in October. At 20°N, advection results in a freshening tendency throughout the year, though it is strongest during boreal spring, presumably because of the arrival of the low SSS water from the south.
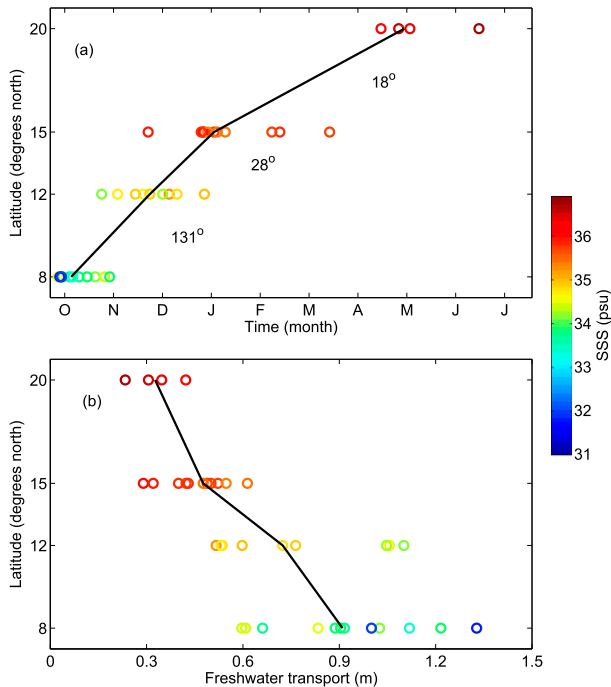
FIG. 8. (a) Calendar day of the minimum SSS at each PIRATA mooring location (circles, with color indicating the minimum SSS). Black lines connect the median calendar day at each location. Numbers between mooring locations show the predicted angle (measured counterclockwise from east) that the low SSS front must make with a line of constant latitude, averaged between those locations. (b) As in (a), but for the horizontal freshwater transport in the upper 20 m associated with the observed drop in SSS.

The arrival of the low SSS front, defined as the day on which observed SSS reaches its minimum value, consistently occurs during late September and October at 8°N, though the range of the minimum SSS values is about 3 psu (Fig. 8a). We choose to use observed SSS to define the front because of uncertainties in the estimation of the advection-driven SSS from the salinity budget residual. There is progressively more spread in the arrival day of the front from 8° to 15°N, but the range of minimum SSS values decreases northward. The increasing variability of the arrival date, from south to north, can likely be explained by the time-integrated effects of year-to-year changes in the mean northward current speed and possibly eddy activity in the NECC, which may affect the location and intensity of the low SSS water at 8°N and hence the time required to reach higher latitudes.

With knowledge of the observed surface currents between 8° and 12°N and the time required for the low SSS front to travel between the moorings, the orientation of the front in the x–y plane can be predicted (see appendix A for details). Given the observed surface currents, it is found that the front must have an average

angle of 131° from a line of constant latitude, measured counterclockwise from the east. It is difficult to determine whether this angle is realistic, given the presence of strong eddy variability in the NECC at that latitude (Fig. 1; Johns et al. 1990), though it seems unlikely that such a large angle would exist in a time-mean sense. Instead, it is possible that northward advection of the low SSS water from 8°N actually begins prior to the date of the minimum SSS, especially since there is normally a broad minimum in SSS at 8°N (Fig. 7a). Earlier northward advection would increase the travel time between moorings and thus decrease the required front angle (see appendix A). Between 12° and 15°N and between 15° and 20°N, much smaller front angles are estimated (Fig. 8a). The slight northeast to southwest tilt (18°–28°) is generally consistent with observations from *Aquarius*, which show a gradual tilt of lines of constant SSS toward the northeast from about 40°W to the African coast (Fig. 1). This tilt introduces a westward component to the low-salinity front's northward movement since the mean surface currents are northwestward.

Consistent with the northward decrease in year-to-year variability of the low-salinity water's minimum SSS (Fig. 8a), there is also a northward decrease in interannual variability of horizontal freshwater transport (Fig. 8b). Freshwater transport in the upper 20 m ranges from 0.6 to 1.3 m at 8°N, decreasing to 0.2–0.4 m at 20°N. On average there is a 70% reduction in horizontal freshwater transport between 8° and 20°N. There is also a northward decrease in freshwater transport in the 20–40- and 40–60-m layers, though as expected, the total transport is lower (Fig. 9). The northward decrease in transport between 8° and 20°N is consistent with a northward increase in E–P in the same latitude band and the mixing of higher-salinity water from beneath the mixed layer.

To assess the impact of vertical mixing on the low-salinity water as it moves northwestward between moorings, we first consider the variations in surface buoyancy flux $[B_0 = \beta \rho S(E - P) - \alpha c_p^{-1} Q]$ and wind friction velocity cubed $[u_*^3 = (\tau/\rho)^{3/2}]$ between each mooring pair (8° and 12°N, 12° and 15°N, and 15° and 20°N), averaged during the periods when the low SSS water is located between those moorings (Fig. 10a). In these expressions, α and β are the coefficients of thermal expansion and haline contraction, respectively; ρ is the density of seawater; Q is the surface heat flux; E is evaporation; P is precipitation; and τ is the wind stress magnitude. The friction velocity cubed and surface buoyancy flux have been shown to be proportional to mixing at the base of the mixed layer (Kraus and Turner 1967; Niiler and Kraus 1977). The terms vary in phase between 8° and 20°N; the friction velocity peaks between 12° and 15°N, where the surface buoyancy flux is largest
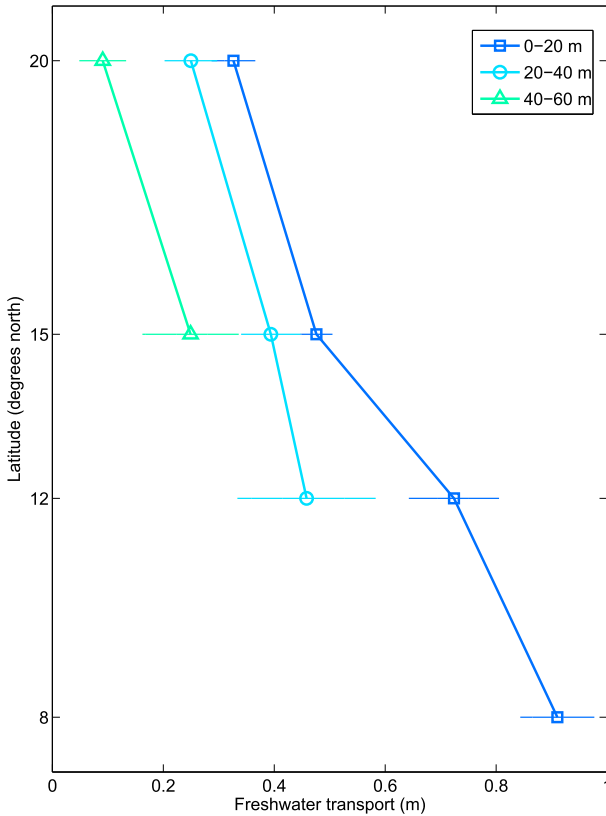
FIG. 9. Median values (1998–2013) of the horizontal freshwater transport at each PIRATA mooring location, calculated from the observed drop in SSS (calendar days and minimum values of SSS after the drop are shown in Fig. 8). Shown are the transport in the upper 20 m (dark blue squares), 20–40-m depth range (light blue circles), and 40–60-m depth range (green triangles). Horizontal lines indicate one standard error. Transports in the 20–40- and 40–60-m ranges were found to decrease southward from 12° and 15°N, respectively, and are therefore not shown. The cause of the southward decreases is likely a southward increase in subsurface salinity, combined with a northward increase in mixed layer depth (i.e., the low SSS water is mixed downward from approximately 20 m at 8°N to 60 m at 15°N).

(Fig. 10a). The changes in latitude and season both contribute to the changes in wind and buoyancy forcing. The maxima in friction velocity and buoyancy forcing in the 12°–15°N band are consistent with the arrival of the low SSS front in that region during December–January, when winds are strong and surface solar radiation is at a seasonal minimum. The smaller friction velocity and buoyancy flux to the north and south are due to the presence of weaker winds and stronger solar radiation during the passage of the front in boreal fall (8°–12°N) and spring (15°–20°N).

To estimate the impacts of changes in the surface buoyancy flux and winds on the vertical mixing rate, we simplify Niiler and Kraus's (1977) expression for entrainment velocity by setting the vertical current shear
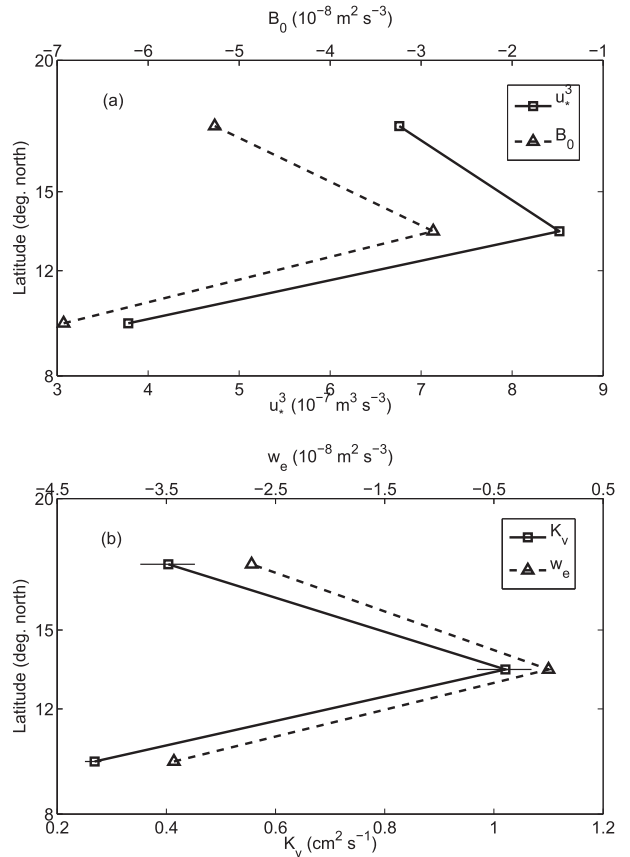

FIG. 10. (a) Surface buoyancy flux (triangles, with positive values indicating a tendency to increase surface density and hence vertical mixing) and wind friction velocity cubed (squares) averaged between each mooring pair (8°–12°N, 12°–15°N, and 15°–20°N) during the time when the low SSS front was located between the moorings. (b) As in (a), but for a term proportional to the wind plus buoyancy-induced vertical mixing (triangles) and the vertical turbulent mixing coefficient for salt (squares). Horizontal lines in (b) indicate one standard error of the vertical mixing coefficient.

to zero and neglecting penetrative solar radiation. The resultant expression is

$$w_e \propto \frac{2u_*^3}{h} + B_0. \qquad (6)$$

Here, w_e is the mixing rate expressed in terms of an entrainment velocity, and h is the mixed layer depth. Because entrainment can only thicken the mixed layer, values of w_e that are less than zero are set to zero. A similar expression was used by Foltz et al. (2013) to estimate vertical mixing in the northeastern tropical Atlantic.

The sum of the buoyancy flux and wind forcing [(6)] explains the latitudinal distribution of the vertical mixing coefficient very well (Fig. 10b; appendix B describes the methodology used to calculate the mixing coefficient averaged between mooring pairs). Both have a sharp

maximum between 12° and 15°N. Based on the vertical mixing coefficients and the observed $E-P$ and freshwater transport, we find that vertical mixing explains 134%, 52%, and 22% of the freshwater loss in the upper 20 m in the 8°–12°N, 12°–15°N, and 15°–20°N regions, respectively. Another way to interpret the high percentage above 100% between 8° and 12°N is that vertical mixing tends to decrease the transport at a rate that is 34% larger than the rate of increase due to E–P. The decrease in relative importance of vertical mixing with latitude can be explained by the increasing importance of $E-P$. The maximum in K_v in the 12°–15°N band is consistent with the arrival of the low-salinity water in that latitude band during December–January, when winds are strong and the surface buoyancy flux is large. The values of the mixing coefficient K_v of 0.3–1.0 cm^2 s^{-1} are consistent with, though at the lower end of, the annual range of K_v for temperature in the same latitude bands along 23°W. Foltz et al. (2013) found annual ranges of K_v for temperature of 0–3.3 cm^2 s^{-1} in the ITCZ region (3°–8°N, 23°W) and 0.3–4.1 cm^2 s^{-1} in the trade wind region (15°–25°N, 23°W).

Given the consistency of the vertical mixing coefficients for temperature and salinity between 8° and 20°N, it is interesting to compare the damping time scales for SST and SSS. Observed damping rates for SST in the tropical North Atlantic are about 10 W m^{-2} K^{-1} (Park et al. 2005). Using a surface layer thickness of 20 m, a rough estimate of the time required for SST to decrease 70% is 104 days. In contrast, 210 days are required for SSS to increase 70% from 8° to 20°N. The longer damping time for SSS is likely because of the absence of negative surface heat flux feedback that is present for SST. Instead, SSS appears to be damped primarily by vertical turbulent mixing and possibly horizontal eddy advection. The small damping coefficient for salinity has important implications for SSS variability in the tropical North Atlantic, since changes in freshwater input in the equatorial Atlantic can be transmitted efficiently to remote areas downstream.

c. Interannual variability

Measurements from the PIRATA moorings along 38°W revealed a consistent seasonality in the arrival of the freshwater front and considerable interannual variability in its strength (Figs. 7, 8). To investigate interannual variations in more detail, we define the low SSS front's strength at a given mooring location in a given year as the minimum SSS recorded by that mooring in that year after application of a 5-day running-mean filter. To look at possible links to ocean circulation, we also calculate the near-surface currents from the drifter–altimeter synthesis product, averaged
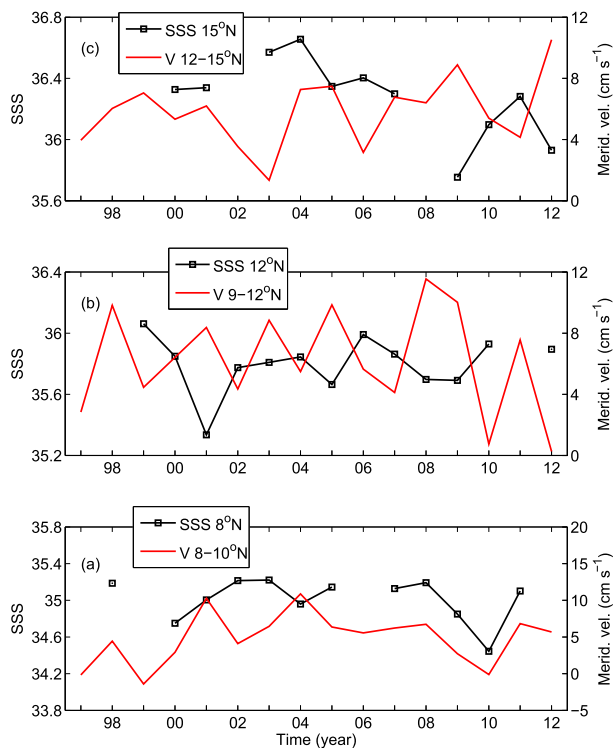

FIG. 11. Minimum SSS observed at each mooring location during each calendar year (black squares) and northward surface velocity averaged in the latitude ranges indicated and centered on the mooring longitude and the day of the minimum SSS (red). Shown are the (a) 8°, (b) 12°, and (c) 15°N mooring locations. Note that (a) is the bottom panel.

during September–October at 8°N, October–November at 12°N, and December–January at 15°N. These 2-month periods generally correspond to the months before and during the arrival of the SSS front at each location (Fig. 8a).

At 8°N, the strength of the drop in SSS varies in phase with meridional velocity averaged between 8° and 10°N (i.e., weaker northward currents tend to occur during years with lower SSS) during 1998, 2000–01, and 2007–11, but out of phase during 2002–05 (Fig. 11a). At this location the velocity has been averaged between 8° and 10°N to avoid the strongest eddy-induced currents to the south of the mooring, which may contaminate the September–October means. Overall, there is a positive correlation of 0.5 between the strength in the SSS drop and meridional velocity, which is significant at the 90% level. The positive correlation is consistent with the location of the 8°N mooring in the southern half of the zonal band of lowest SSS during boreal fall (Fig. 1b). With this positioning, anomalous northward currents tend to push the low SSS water farther away to the north and thus increase SSS and conversely for anomalous

southward currents. The strength of the SSS drop at 8°N, 38°W is not significantly correlated with zonal current speed west of 38°W, suggesting that the strength of the NECC is not an important factor for controlling SSS variability at 8°N, 38°W.

At the 12° and 15°N moorings, meridional currents to the south of the moorings tend to vary out of phase with SSS at the moorings (Figs. 11b,c). The correlation is −0.6 at each location, which is significant at the 95% level. The out-of-phase relationships suggest that stronger northward currents result in the arrival of fresher water from the south. The lower SSS could be because of the advection of more freshwater from the south or a reduction in travel time of the low SSS water to the mooring, resulting in less evaporation and vertical mixing during transit to the mooring and hence lower SSS. Whatever the mechanism, these results suggest that ocean circulation may drive a significant portion of interannual variability of SSS as far north as 15°N in the Atlantic.

5. Summary and discussion

Observations from *Aquarius* and Argo show a strong decrease in SSS in the western tropical North Atlantic (5°–10°N, 30°–50°W) during boreal summer and fall. West of 40°W this freshening is driven primarily by eastward transport of freshwater from the Amazon, while to the east it is forced mainly by an increase in precipitation as the ITCZ moves northward. During boreal fall through spring, low-salinity water from the equatorial Atlantic is dispersed northward to 20°N, consistent with a strengthening of the mean northward surface currents during boreal fall and winter.

Measurements from a meridional line of moorings in the central tropical North Atlantic (38°W) support the conclusions drawn from satellite data and Argo profiles. The moorings show a pronounced decrease in SSS at 8°N during boreal fall that results from eastward advection of low SSS water from the Amazon and an increase in rainfall as the ITCZ moves northward. The northward progression of the low SSS water generates abrupt drops in SSS of 1–2.5 psu at 12°N, 0.5–1 psu at 15°N, and ~0.5 psu at 20°N, usually within a period of one to two weeks. The travel speed of the low SSS water between the 12° and 20°N moorings is consistent with advection by the mean currents and a southwest to northeast tilt of the front's leading edge. The transport mechanism between 8° and 12°N is less clear and may involve a combination of the northward progression of the ITCZ and meridional advection.

As the low SSS water moves northward, it is damped by surface evaporation and vertical turbulent mixing. As a result, in the upper 20 m, northward freshwater transport

associated with the low SSS water's passage amounts to 0.7 m at 12°N, 0.5 m at 15°N, and 0.3 m at 20°N on average. We estimate that vertical mixing accounts for 52% and 22% of the loss of freshwater between 12° and 15°N and 15° and 20°N, respectively, with the remainder removed by the surface moisture flux. Between 8° and 12°N, the freshwater transport decreases northward despite an input of freshwater from the surface. As a result, vertical mixing tends to decrease the transport at a rate that is 34% larger than the rate of increase due to the surface flux.

Pronounced interannual variations in the low SSS front's strength were observed during 1998–2012 based on the mooring data, consistent with the modeling results of Ferry and Reverdin (2004). At 8°N, the SSS tends to vary in phase with the strength of the northward currents, meaning that anomalously strong northward flow pushes the low SSS water farther north than normal, thus resulting in higher SSS at 8°N. At 12° and 15°N, SSS varies out of phase with northward velocity to the south. The interpretation is that stronger northward flow transports more low SSS water from the south, decreasing SSS at the mooring. These results point to the importance of ocean circulation for generating interannual variations of SSS as far north as 15°N. Changes in evaporation, rainfall, and river runoff appear to play much smaller roles, though additional analysis is needed because of the shortness of the mooring records.

Measurements from the PIRATA moorings revealed the passage of a sharp zonally oriented SSS front as the low SSS water moves northward each year. The generation of the front is likely driven by the combination of sharp meridional gradients of rainfall in the equatorial region and the eastward advection of Amazon freshwater, both of which tend to generate zonally oriented fronts. Similar northward movement of SST fronts is not observed in the tropics since the surface heat flux is generally more evenly distributed spatially compared to $E-P$ and river discharge, and the surface heat flux damps SST anomalies. An important consequence is that low SSS water can travel larger distances and affect SSS farther from its sources compared to SST. Indeed, horizontal advection of low SSS water from the equatorial region has been recognized as an important mechanism for barrier layer formation in the subtropics (Sprintall and Tomczak 1992; Sato et al. 2006; Mignot et al. 2007). Another consequence is that it may be more difficult to interpret changes in SSS in a given region compared to changes in SST, since horizontal SSS transport can occur over much larger distances. For example, we found that the damping rate for SSS is about half that of SST in the central tropical North Atlantic.

As the length of the satellite SSS record expands, more accurate quantification of submonthly to interannual

variability of SSS transport will be possible. Already, satellite measurements are beginning to reveal important spatial and temporal variations of SSS that previously were undetectable (Lee et al. 2012; Tzortzi et al. 2013; Grodsky et al. 2014b). Continued measurements from Argo floats and moorings are also needed for improved quantification of the depth-dependence of freshwater transport and more accurate estimates of the vertical flux of salt from turbulent mixing.

APPENDIX A

SSS Front Angle

To test the hypothesis that the low-salinity front is simply advected by the mean currents, we consider the observed upper-ocean velocity from the weekly drifter synthesis product. For the simple case in which a zonally oriented band of low-salinity water forms that is then advected northward by the mean currents, a comparison of the mean meridional current speed to the observed time required for the low-salinity front to travel between the PIRATA moorings could be used to test the hypothesis. However, since zonal advection is also likely to contribute (i.e., the low-salinity front is not purely zonal and the zonal component of velocity is nonzero), we instead consider an expression for the average angle that the salinity front makes with a line of constant latitude, assuming that the front is advected by the mean near-surface currents.

From Fig. A1, it is apparent that $\cos\theta_f = d_f/d$, $\cos\theta_u = (d/t)/|\mathbf{v}|$, and $\theta_f = \sin^{-1}(u/|\mathbf{v}|) - \theta_u$. Here, θ_f is the angle the front makes with a line of constant latitude (measured counterclockwise from the east); d_f is the perpendicular distance from the southern mooring to the front; d is the distance between moorings; t is the time it takes from the front to travel between moorings; $\mathbf{v}$ is the observed near-surface velocity averaged between moorings and during the time period of the SSS front's movement between moorings; u is observed zonal velocity; and θ_u is as defined in Fig. A1. Combining these equations and using trigonometric identities for $\cos[\sin^{-1}(x)]$, $\sin[\cos^{-1}(x)]$, and $\cos(x + y)$, where x and y are generic quantities, gives

$$\cos^2\theta_f = \frac{u^2}{|\mathbf{v}|^2}\left[\left(1 - R\sqrt{1 - \frac{u^2}{|\mathbf{v}|^2}}\right)^2 + R^2\frac{u^2}{|\mathbf{v}|^2}\right]^{-1}, \quad \text{(A1)}$$
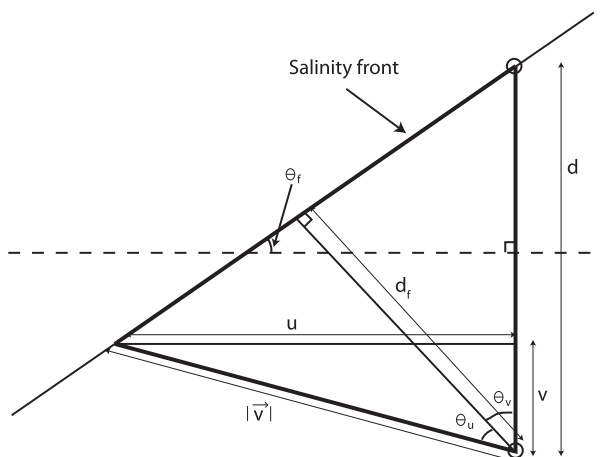
$$R = \frac{d}{t|\mathbf{v}|}. \quad \text{(A2)}$$

FIG. A1. Diagram illustrating the methodology used to calculate the angle between the low-salinity front and a line of constant latitude θ_f. Black circles indicate positions of PIRATA moorings, and u and v are observed zonal and meridional velocity, respectively, averaged between the moorings.

Here, R is the ratio of the observed speed of the front between moorings to the observed surface current speed. From (A1), if the meridional surface current is zero ($v = 0$), $\cos^2\theta_f = 1/[1 + d^2/(t^2u^2)]$, so that θ_f decreases for increasing u, all other variables remaining constant. This is consistent with a front with a smaller tilt requiring a stronger zonal current to advect the front to the next mooring in a given amount of time. If $|v| \gg |u|$, then as d/t approaches $|\mathbf{v}|$, θ_f goes to zero, consistent with pure meridional advection.

As defined in (A1), θ_f varies between zero (i.e., zonally oriented front) and 90° (i.e., meridionally oriented). The orientation of the front (i.e., northwest to southeast or northeast to southwest) depends on the average speed of the front between moorings ($s_f = d/t$) and the meridional current speed v. For $s_f/v > 1$ (i.e., travel speed of the front exceeds the observed meridional velocity) and $u > 0$ (i.e., eastward flow), the front must be oriented northwest to southeast so that the observed eastward flow pushes the tilted front toward the mooring faster than the northward flow would on its own. Similarly, the orientation of the front can be determined for cases when $s_f/v > 1$ and $u < 0$ and when $s_f/v < 1$.

APPENDIX B

Vertical Mixing Coefficient

As low-salinity water moves northward from the equatorial Atlantic, it is modified primarily by the air–sea moisture flux, horizontal eddy advection, and vertical

mixing. The vertical mixing coefficient of salinity for a surface layer can be estimated as

$$K_v = (hM) \bigg/ \left(\frac{\partial S}{\partial z}\right). \tag{B1}$$

Here, h is the mixed layer depth; M is the rate of change of salinity in the layer due to vertical turbulent mixing; and $\partial S/\partial z$ is the vertical gradient of salinity at the base of the mixed layer. The quantity K_v is calculated using the time series of analyzed SSS at each PIRATA mooring location, together with Argo subsurface salinity and satellite-based evaporation and precipitation averaged between the moorings. The methodology is as follows.

We calculate $\partial S/\partial z$ in (B1) using the difference between Argo salinity averaged in the mixed layer and salinity averaged between depths of h and $h + 20$. The M term is calculated as $\Delta S/\Delta t$, where ΔS is the change in the surface layer salinity of the low-salinity water due to vertical mixing during its transit between mooring pairs, and Δt is the observed time for the low SSS front to travel between moorings. The ΔS term can be expressed as

$$\Delta S = \frac{(V_s - V_n)[\rho_f - \rho(1 - S_{-h})]}{\rho h}. \tag{B2}$$

Here, V_n and V_s are the volumes of freshwater added at the northern and southern moorings, respectively, calculated from (5). We calculate ΔS in the upper 20 m between 8° and 12°N and in the upper 50 m between 12° and 15°N and between 15° and 20°N, based on the Argo climatology of h averaged between each mooring pair. To account for the freshwater loss due to the surface moisture flux, we subtract $(E - P)S/h$, integrated in time from the arrival of the low-salinity front at the southern mooring to its arrival at the northern mooring, from S_1 in (5) before computing V_f. The OAFlux evaporation and TRMM precipitation are used for E and P, respectively. Because reliable estimates of horizontal eddy advection are not available, they are not subtracted before computing K_v. Our estimates of K_v can therefore likely be viewed as an upper bound, since eddy advection is expected to cause an increasing tendency in SSS between 12° and 20°N. Since K_v is estimated using a residual method, it implicitly includes contributions from entrainment (i.e., mixed layer deepening). We calculate $\partial S/\partial z$, E, P, and S as the averages in space and time during the low-salinity front's transit between each mooring pair, from the southern mooring to the northern mooring. The estimates of K_v therefore represent mean values between the mooring pairs.

REFERENCES

Balaguru, K., P. Chang, R. Saravanan, L. R. Leung, Z. Xu, M. K. Li, and J.-S. Hsieh, 2012: Ocean barrier layers' effect on tropical cyclone intensification. *Proc. Natl. Acad. Sci. USA,* **109,** 14 343–14 347, doi:10.1073/pnas.1201364109.

Bingham, F. M., G. R. Foltz, and M. J. McPhaden, 2012: Characteristics of the seasonal cycle of surface layer salinity in the global ocean. *Ocean Sci.,* **8,** 915–929, doi:10.5194/os-8-915-2012.

Bourlès, B., and Coauthors, 2008: The PIRATA program: History, accomplishments, and future directions. *Bull. Amer. Meteor. Soc.,* **89,** 1111–1125, doi:10.1175/2008BAMS2462.1.

Coles, V. J., M. T. Brooks, J. Hopkins, M. R. Stukel, P. L. Yager, and R. R. Hood, 2013: The pathways and properties of the Amazon River plume in the tropical North Atlantic Ocean. *J. Geophys. Res.,* **118,** 6894–6913, doi:10.1002/2013JC008981.

Cravatte, S., T. Delcroix, D. X. Zhang, M. J. McPhaden, and J. Leloup, 2009: Observed freshening and warming of the western Pacific warm pool. *Climate Dyn.,* **33,** 565–589, doi:10.1007/s00382-009-0526-7.

Curry, R., B. Dickson, and I. Yashayaev, 2003: A change in the freshwater balance of the Atlantic Ocean over the past four decades. *Nature,* **426,** 826–829, doi:10.1038/nature02206.

Da-Allada, C. Y., G. Alory, Y. du Penhoat, E. Kestenare, F. Durand, and N. M. Hounkonnou, 2013: Seasonal mixed-layer salinity balance in the tropical Atlantic Ocean: Mean state and seasonal cycle. *J. Geophys. Res.,* **118,** 332–345, doi:10.1029/2012JC008357.

Dessier, A., and J. R. Donguy, 1994: The sea surface salinity in the tropical Atlantic between 10°S and 30°N—Seasonal and interannual variations (1977–1989). *Deep-Sea Res.,* **41,** 81–100, doi:10.1016/0967-0637(94)90027-2.

Durack, P. J., S. E. Wijffels, and R. J. Matear, 2012: Ocean salinities reveal strong global water cycle intensification during 1950 to 2000. *Science,* **336,** 455–458, doi:10.1126/science.1212222.

Fairall, C. W., E. F. Bradley, J. E. Hare, A. A. Grachev, and J. B. Edson, 2003: Bulk parameterization of air–sea fluxes: Updates and verification for the COARE algorithm. *J. Climate,* **16,** 571–591, doi:10.1175/1520-0442(2003)016<0571:BPOASF>2.0.CO;2.

Ferry, N., and G. Reverdin, 2004: Sea surface salinity interannual variability in the western tropical Atlantic: An ocean general circulation model study. *J. Geophys. Res.,* **109,** C05026, doi:10.1029/2003JC002122.

Ffield, A., 2007: Amazon and Orinoco River plumes and NBC rings: Bystanders or participants in hurricane events? *J. Climate,* **20,** 316–333, doi:10.1175/JCLI3985.1.

Foltz, G. R., and M. J. McPhaden, 2008: Seasonal mixed layer salinity balance of the tropical North Atlantic Ocean. *J. Geophys. Res.,* **113,** C02013, doi:10.1029/2007JC004178.

——, and ——, 2009: Impact of barrier layer thickness on SST in the central tropical North Atlantic. *J. Climate,* **22,** 285–299, doi:10.1175/2008JCLI2308.1.

——, S. A. Grodsky, J. A. Carton, and M. J. McPhaden, 2004: Seasonal salt budget of the northwestern tropical Atlantic Ocean along 38°W. *J. Geophys. Res.,* **109,** C03052, doi:10.1029/2003JC002111.

——, C. Schmid, and R. Lumpkin, 2013: Seasonal cycle of the mixed layer heat budget in the northeastern tropical Atlantic Ocean. *J. Climate,* **26,** 8169–8188, doi:10.1175/JCLI-D-13-00037.1.

Grodsky, S. A., J. A. Carton, and F. O. Bryan, 2014a: A curious local surface salinity maximum in the northwestern tropical Atlantic. *J. Geophys. Res.,* **119,** 484–495, doi:10.1002/2013JC009450.

——, G. Reverdin, J. A. Carton, and V. J. Coles, 2014b: Year-to-year salinity changes in the Amazon plume: Contrasting 2011 and 2012 *Aquarius*/SACD and SMOS satellite data. *Remote Sens. Environ.,* **140,** 14–22, doi:10.1016/j.rse.2013.08.033.

Held, I. M., and B. J. Soden, 2006: Robust responses of the hydrological cycle to global warming. *J. Climate,* **19,** 5686–5699, doi:10.1175/JCLI3990.1.

Hu, C., E. T. Montgomery, R. W. Schmitt, and F. E. Muller-Karger, 2004: The dispersal of the Amazon and Orinoco River water in the tropical Atlantic and Caribbean Sea: Observation from space and S-PALACE floats. *Deep-Sea Res.,* **51,** 1151–1171, doi:10.1016/j.dsr2.2004.04.001.

Johns, W. E., T. N. Lee, F. A. Schott, R. J. Zantopp, and R. H. Evans, 1990: The North Brazil Current retroflection: Seasonal structure and eddy variability. *J. Geophys. Res.,* **95,** 22 103–22 120, doi:10.1029/JC095iC12p22103.

Johnson, E. S., G. S. E. Lagerloef, J. T. Gunn, and F. Bonjean, 2002: Surface salinity advection in the tropical oceans compared with atmospheric freshwater forcing: A trial balance. *J. Geophys. Res.,* **107,** 8014, doi:10.1029/2001JC001122.

Kraus, E. B., and J. S. Turner, 1967: A one-dimensional model of the seasonal thermocline. *Tellus,* **19,** 98–105, doi:10.1111/j.2153-3490.1967.tb01462.x.

Lee, T., G. Lagerloef, M. M. Gierach, H.-Y. Kao, S. Yueh, and K. Dohan, 2012: *Aquarius* reveals salinity structure of tropical instability waves. *Geophys. Res. Lett.,* **39,** L12610, doi:10.1029/2012GL052232.

Lumpkin, R., and S. L. Garzoli, 2005: Near-surface circulation in the tropical Atlantic Ocean. *Deep-Sea Res. I,* **52,** 495–518, doi:10.1016/j.dsr.2004.09.001.

——, and ——, 2011: Interannual to decadal variability in the southwestern Atlantic's surface circulation. *J. Geophys. Res.,* **116,** C01014, doi:10.1029/2010JC006285.

——, and G. C. Johnson, 2013: Global ocean surface velocities from drifters: Mean, variance, El Niño–Southern Oscillation response, and seasonal cycle. *J. Geophys. Res. Oceans,* **118,** 2992–3006, doi:10.1002/jgrc.20210.

Maes, C., J. Picaut, and S. Belamari, 2002: Salinity barrier layer and onset of El Niño in a Pacific coupled model. *Geophys. Res. Lett.,* **29,** 2206, doi:10.1029/2002GL016029.

McPhaden, M. J., and G. R. Foltz, 2013: Intraseasonal variations in the surface layer heat balance of the central equatorial Indian Ocean: The importance of zonal advection and vertical mixing. *Geophys. Res. Lett.,* **40,** 2737–2741, doi:10.1002/grl.50536.

Mignot, J., C. de Boyer Montégut, A. Lazar, and S. Cravatte, 2007: Control of salinity on the mixed layer depth in the world ocean: 2. Tropical areas. *J. Geophys. Res.,* **112,** C10010, doi:10.1029/2006JC003954.

——, A. Lazar, and M. Lacarra, 2012: On the formation of barrier layers and associated vertical temperature inversions: A focus on the northwestern tropical Atlantic. *J. Geophys. Res.,* **117,** C02010, doi:10.1029/2011JC00743.

Muller-Karger, F. E., C. R. McClain, and P. L. Richardson, 1988: The dispersal of the Amazon's water. *Nature,* **333,** 56–58, doi:10.1038/333056a0.

Niiler, P. P., and E. B. Kraus, 1977: One-dimensional models of the upper ocean. *Modelling and Prediction of the Upper Layers of the Ocean,* E. B. Kraus, Ed., Pergamon, 143–172.

Pailler, K., B. Bourles, and Y. Gouriou, 1999: The barrier layer in the western tropical Atlantic Ocean. *Geophys. Res. Lett.,* **26,** 2069–2072, doi:10.1029/1999GL900492.

Park, S., C. Deser, and M. A. Alexander, 2005: Estimation of the surface heat flux response to sea surface temperature anomalies over the global oceans. *J. Climate,* **18,** 4582–4599, doi:10.1175/JCLI3521.1.

Qu, T. D., S. Gao, and I. Fukumori, 2011: What governs the North Atlantic salinity maximum in a global GCM? *Geophys. Res. Lett.,* **38,** L07602, doi:10.1029/2011GL046757.

Reverdin, G., E. Kestenare, C. Frankignoul, and T. Delcroix, 2007: Surface salinity in the Atlantic Ocean (30°S–50°N). *Prog. Oceanogr.,* **73,** 311–340, doi:10.1016/j.pocean.2006.11.004.

Sato, K., T. Suga, and K. Hanawa, 2006: Barrier layers in the subtropical gyres of the world's oceans. *Geophys. Res. Lett.,* **33,** L08603, doi:10.1029/2005GL025631.

Sprintall, J., and M. Tomczak, 1992: Evidence of the barrier layer in the surface layer of the tropics. *J. Geophys. Res.,* **97,** 7305–7316, doi:10.1029/92JC00407.

Terray, L., L. Corre, S. Cravatte, T. Delcroix, G. Reverdin, and A. Ribes, 2012: Near-surface salinity as nature's rain gauge to detect human influence on the tropical water cycle. *J. Climate,* **25,** 958–977, doi:10.1175/JCLI-D-10-05025.1.

Tzortzi, E., S. A. Josey, M. Srokosz, and C. Gommenginger, 2013: Tropical Atlantic salinity variability: New insights from SMOS. *Geophys. Res. Lett.,* **40,** 2143–2147, doi:10.1002/grl.50225.

Vellinga, M., and P. Wu, 2004: Low-latitude freshwater influence on centennial variability of the Atlantic thermohaline circulation. *J. Climate,* **17,** 4498–4511, doi:10.1175/3219.1.

Vialard, J., and P. Delecluse, 1998: An OGCM study for the TOGA decade. Part II: Barrier layer formation and variability. *J. Phys. Oceanogr.,* **28,** 1089–1106, doi:10.1175/1520-0485(1998)028<1089:AOSFTT>2.0.CO;2.

Wang, C. Z., S. F. Dong, and E. Muñoz, 2010: Seawater density variations in the North Atlantic and the Atlantic meridional overturning circulation. *Climate Dyn.,* **34,** 953–968, doi:10.1007/s00382-009-0560-5.

Wentz, F. J., L. Ricciardulli, K. Hilburn, and C. Mears, 2007: How much more rain will global warming bring? *Science,* **317,** 233–235, doi:10.1126/science.1140746.

Yu, L. S., 2011: A global relationship between the ocean water cycle and near-surface salinity. *J. Geophys. Res.,* **116,** C10025, doi:10.1029/2010JC006937.

——, and R. A. Weller, 2007: Objectively analyzed air–sea heat fluxes for the global ice-free oceans (1981–2005). *Bull. Amer. Meteor. Soc.,* **88,** 527–539, doi:10.1175/BAMS-88-4-527.

Zhou, Y. P., K.-M. Xu, Y. C. Sud, and A. K. Betts, 2011: Recent trends of the tropical hydrological cycle inferred from Global Precipitation Climatology Project and International Satellite Cloud Climatology Project data. *J. Geophys. Res.,* **116,** D09101, doi:10.1029/2010JD015197.